Volume and Enthalpy Changes of Proton Transfers in the Bacteriorhodopsin Photocycle Studied by Millisecond Time-Resolved Photopressure Measurements[†]

Yan Liu,*[,‡] Gregory J. Edens,[§] Joseph Grzymski,[||] and David Mauzerall*[,⊥]

Department of Chemistry and Biochemistry, Arizona State University, Tempe, Arizona 85287, Complete Analysis Laboratories, 1259 U.S. Highway 46, Building 4C, Parsippany, New Jersey 07054, Division of Earth and Ecosystem Sciences, Desert Research Institute, Reno, Nevada 89512, and Rockefeller University, 1230 York Avenue, New York, New York 10065-6399

Received January 28, 2008; Revised Manuscript Received April 25, 2008

ABSTRACT: The volume and enthalpy changes associated with proton translocation steps during the bacteriorhodopsin (BR) photocycle were determined by time-resolved photopressure measurements. The data at 25 °C show a prompt increase in volume followed by two further increases and one decrease to the original state to complete the cycle. These volume changes are decomposed into enthalpy and inherent volume changes. The positive enthalpy changes support the argument for inherent entropy-driven late steps in the BR photocycle [Ort, D. R., and Parson, W. M. (1979) Enthalpy changes during the photochemical cycle of bacteriorhodopsin. *Biophys. J. 25*, 355−364]. The volume change data can be interpreted by the electrostriction effect as charges are canceled and formed during the proton transfers. A simple glutamic acid−glutamate ion model or a diglutamate−arginine−protonated water charge-delocalized model for the proton-release complex (PRC) fit the data. A conformational change with a large positive volume change is required in the slower rise (M → N of the optical cycle) step and is reversed in the decay (N → O → BR) steps. The large variation in the published values for both the volume and enthalpy changes is greatly ameliorated if the values are presented per absorbed photon instead of per mole of BR. Thus, it is the highly differing assumptions about the quantum or reaction yields that cause the variations in the published results.

Bacteriorhodopsin (BR)[1] is one of a large class of seven-helix membrane proteins that function as signal transducers in a wide variety of organisms (*2*). Their structure seems to be delicately balanced such that photoisomerization of a retinal pigment in the case of the rhodopsins, or the binding of substrate in the case of receptor proteins, leads to conformational changes. These trigger further events in a cascade. Such properties alone would be sufficient to justify the large amount of work on BR, but in addition, it is a molecular machine. Whereas the other retinal proteins are sensors, which essentially trigger preordained responses to absorbed photons, BR uses the energy of the photon to pump protons (chloride ions in the case of halorhodopsin) across a membrane and against a gradient. BR is a 26 kDa single-peptide chain that transforms the energy of the absorbed photon to chemical potential energy. The photosynthetic reaction center is far more efficient in converting photon to chemical energy but requires three peptides and more than one-half dozen pigment and redox molecules.

The proton path through BR is now known in some detail (*3*). The highly successful X-ray crystallographic work, including several intermediates in the photocycle (for reviews, see refs *4–7*) has been a breakthrough. Combined with the extensive optical spectroscopic measurements (*8–12*), this has led to models of six or seven reversible reactions and one or two irreversible steps (Scheme 1). The kinetics and molecular composition of these steps are known; however, their energetics are far less well-known. The early work of Ort and Parson (*1, 13, 14*) on enthalpy and volume changes during the photocycle suggested that the last steps in the cycle were entropy-driven because a large positive enthalpy was found for these steps. Further efforts using differing methodologies have not addressed these observations directly and have produced a highly variable set of data. Here we show that this variability is much reduced when the data are presented per absorbed photon rather than per mole of BR. Most of the variability thus relates to differing assumptions about the quantum or reaction yields. The work presented here supports some of the results of Ort and Parson with a more robust methodology. The inherent volume changes are assigned to the charge neutralization and formation on proton transfer in the various steps. Estimation of these electrostrictive contributions to the volume changes leaves a large positive volume change on an intermediate reaction and its reversal on the final step. We associate this

[†] We thank the National Institutes of Health for support via Grant GM 25693-22.

* To whom correspondence should be addressed. D.M.: Rockefeller University, 1230 York Ave., New York, NY 10065-6399; e-mail, mauzera@.rockefeller.edu. Y.L.: e-mail, yan_liu@asu.edu.

[‡] Arizona State University.

[§] Complete Analysis Laboratories.

[||] Desert Research Institute.

[⊥] Rockefeller University.

[1] Abbreviations: BR, bacteriorhodopsin; FTIR, Fourier transform infrared spectroscopy; CAPS, 3-(cyclohexylamino)-1-propanesulfonic acid; HPLC, high-pressure liquid chromatography; PRC, proton-release complex; PM, purple membrane, aggregated form of BR; S/N, signal-to-noise; Tris, tris(hydroxymethyl)amine buffer.

10.1021/bi800158x CCC: $40.75
Published on Web 06/26/2008

Scheme 1: BR Photocycle

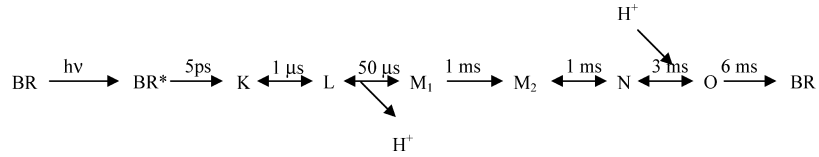

change with the tilt of helix F observed by Dencher et al. (*15*), Subramaniam et al. (*16*), and Radzwill et al. (*17*).

MATERIALS AND METHODS

Sample Preparation. Halobacterium salinarium was grown, and purple membrane patches containing BR were isolated, according to literature protocols (*18*). The purple membrane samples were stored at 4 °C in a 30% sucrose solution. Prior to each use, an aliquot of the purple membrane sample was washed with doubly distilled water, followed by centrifugation twice at 17000 rpm for 30 min, washed with the desired buffer solution once, and finally resuspended in the buffer solution. Following a mild sonication for 2 min, the resulting purple membrane was light adapted by illumination under a lamp for 20 min. Immediately following light adaptation, the optical density of the purple membrane suspension was measured and adjusted to ~0.25 at 585 nm in a 0.1 cm quartz cuvette, corresponding to ~43 μM BR. The purple membrane sample was deaerated under vacuum immediately before being injected into the photopressure cell. This allowed the interfacial film of air in the filled cell to dissolve, decreasing its compressibility. Both 10 mM Tris and potassium phosphate were used as the buffer in the pH range of 7−8.5. For each photopressure experiment, the calorimetric reference (Sheaffer jet black ink) matched in absorbance at 585 nm to that of the purple membrane sample was measured in the same medium as the sample to calibrate the instrument response and provide the impulse response for the signal deconvolution.

Photopressure Experiments. The millisecond time-resolved photopressure measurements were performed with a novel pressure cell. The details of this cell, the methodology, and the verification of its results have been published previously (*19, 20*). The thickness of sample in the cell was 2.1 mm, and the diameter was 17.5 mm. The temperature was kept constant within ±0.01 °C by circulating a thermostated 10:1 water/ethylene glycol mixture.

The laser pulse with a width of 1 μs, peak at 585 nm, was generated from a flash lamp-pumped dye laser (Candela). A 0.1 mM rhodamine 6G solution in HPLC-grade methanol was used as the laser dye. The laser beam was truncated by a 5 mm diameter aperture and then expanded by a concave lens to fit the diameter of the cell. The energy of the laser beam at the cell position was calibrated by a pyroelectric probe (Laser Precision Corp.) and measured for each pulse by reflecting a small portion of the beam into a silicon energy probe (Laser Precision Corp.). Neutral density filters were inserted into the laser beam to adjust the pulse energy flux into the sample cell within the range of 0.16−0.24 mJ/cm^2, corresponding to ~1 × 10^{-9} Einstein/cm^2.

Contrary to opinions in the literature, a long excitation pulse does not necessarily favor multiple excitations or product excitation. It is the energy of the flux and the optical cross sections of the reactant and product that determine these effects (*21*). In our case, the flux was such that 10% of the BR was photoexcited. Since the product K has almost the same optical cross section as BR at 585 nm, the Poisson distribution indicates that only 0.5% of the total BR or 5% of K will be re-excited. This fraction will vary with the ratio of the cross sections of products to reactants. Even if the BR moves over a larger area than the reciprocal of the photon flux density during the flash, only 10% of K will be excited. Since the initial quantum yield is ~0.65, the fraction of K excited is 3−6% at most.

The direct volume change measurements were taken with a pressure transducer (Entran Sensors and Electronics, Fairfield, NJ) mounted in the back wall of the photopressure cell. The small ($\Delta V/V \sim 10^{-6}$) volume change of the sample upon laser excitation was converted to a pressure change in the cell by the compressibility of the medium and the cell, which was converted to a voltage signal by the pressure transducer. The voltage signal was amplified 100-fold and was low pass filtered at either 100 or 3K Hz, depending on the time scale of the measurements, to reduce the random noise (Tektronix ADA400A differential preamplifier). The filtered signal was fed into an integrating digitizer (Hewlett-Packard 3458A multimeter) with a variable sweep speed and integration time at sensitivities of 16−21 bits per ±100 mV and recorded with a Hewlett-Packard 340 computer. The laser was fired at a frequency of 0.2 Hz in the line-locked mode with a digital delay/pulse generator (Stanford Research System), and only one of every two laser pulses was used to excite the sample. A shutter blocked the other pulse, and a dark background signal was taken to subtract from the light signal to cancel the residual 60 Hz pick-up, ~5 μV, leaving a residual noise of 0.5 μV. Thus the sample was excited every 10 s, thereby ensuring the BR sample photocycle was completed after each pulse even at the lowest temperature. The signal was usually averaged for 50−100 pulses, reducing the noise to ~50 nV.

Each series of photopressure measurements was conducted within 36 h, and we observed that at the same temperature, for the same purple membrane sample, the photopressure: energy ratio was stable. After 36 h, the magnitude of the signal decreased by only <5%, possibly due to slight sedimentation of the purple membrane patches but not bleaching, because the OD of the sample was checked after the experiment, and no noticeable change was observed.

DATA ANALYSIS

A good reference material for the photopressure measurement must undergo no photoreaction and release all the energy of the absorbed photon as heat to the medium within the instrument response time. Some of this response time is inherent in the transducer (20 μs), and some is from filtering in the electronics. The photopressure signal from the reference (P_{REF}) can be expressed as

$$P_{REF} = n\frac{F\alpha' E_{hv}}{\kappa} I(t), \quad n = E_0(1 - 10^{-A}) \tag{1}$$

where E_0 is photon flux, A is the absorbance of the solution in the cell (0.21 cm × OD/cm), n is the number of photons absorbed, F is the sensitivity of the pressure transducer, α' equals thermal expansivity/(heat capacity × density), κ is the compressibility, $I(t)$ is the impulse response of the instrument, and E_{hv} is the energy per photon. We have determined that the effective compressibility of the cell and transducer is some 10 times that of water (*19*). Thus, the effect of the temperature variation of κ of water is negligible, unlike the case of photoacoustic pressure wave measurements (*22*), and the effective κ can be absorbed into the constant cell sensitivity, F.

For the purple membrane sample, the BR molecules excited by the absorbed photons go through a photocycle, characterized by optical methods, that includes many photointermediates with lifetimes ranging from 500 fs to ~10 ms and returns to the ground-state BR (Scheme 1). The photopressure signal time profile at temperature T, normalized to the reference signal at 25 °C, can be described by the convolution of the impulse or reference response with a linear summation of exponential functions

$$\frac{P_{BR}{}^{T}(t)}{P_{REF}{}^{25}} = \left(\frac{a'^{T}}{a'^{25}E_{hv}}\right)\left(A_0 + \sum_i A_i e^{-t/\tau_i}\right) I(t) \tag{2}$$

where the time constant τ_i represents the lifetime of the intermediates and the amplitude A_i of the components includes both the enthalpy and volume changes of the reactions (see eq 3). α'^{T} refers to the thermal expansivity of the medium at temperature T. Data were collected on three or four different time scales (500 channels at 20 μs to 5 ms per channel), to adequately sample the response. The deconvolutions were done by reiterative nonlinear least-squares fitting of the data. The convolutions used an exact equation, not the linearized form, so results are exact as $\tau \rightarrow 0$. The results were checked by a global fit. A global least-squares minimization was done by fitting the observed time course of the photopressure changes (measured at varied temperature and for each temperature on different time scales) with the τ' values of each transition step in eq 2 and replacing the A values with eq 3, thus giving Q and ΔH directly. An empirical equation gave α' as a function of temperature. This increased the errors but gave more confidence in the results.

It is understood that the rate constants are fitting parameters and represent only functions of the actual rate constants. The observed rate constants and apparent amplitudes of consecutive reactions deviate from the true constants when these rate constants are similar in magnitude (*23*). We obtained the true amplitudes by using appropriate relations among the amplitudes, rate constants, and apparent amplitudes. However, only the amplitudes and rate constants of the second and third steps at pH 7 (see below) are sufficiently close that they require a roughly 15% correction. The optical kinetic data are often fit with more complex schemes, but because of a limited S/N ratio, our present data do not require these refinements.

The photopressure data were obtained from both the ink reference and PM sample over several time scales at each temperature. The normalized (eq 2) data were fit by least squares, and the fitting residuals were examined. It was found that a three-exponential function was sufficient to obtain satisfactory fitting at the present S/N ratio. From the analysis, both the amplitudes of the components and the lifetimes were obtained. Each amplitude of signal A_i contains two parts, heat Q_i and volume change ΔV_i (*24*). If we assume the heat released and the volume changes are temperature-independent, we have

$$A_i = \frac{1}{a'^{25}}(\alpha'^{T} Q_i + \Delta V_i)/E_{hv} \tag{3}$$

A plot of A_i versus α'^{T}/α'^{25} will give a linear plot with a slope of Q_i/E_{hv}, and an intercept at $\alpha' = 0$ of $\Delta V_i/\alpha'^{25}E_{hv}$. Therefore, the enthalpy change ($-Q_i$) of the photoreaction and the volume changes (ΔV_i) can be deduced. In this experiment, the energy of the photon (E_{hv}) is 205 kJ/mol (585 nm), and $\alpha'^{25}E_{hv}$ is 22.0 Å^3/photon.

The instantaneous component A_0 involves the BR* → K → L steps, because the lifetime of the K (1 μs) intermediate is shorter than the time resolution of the instrument, ~20 μs. The instantaneous heat Q_0 can be expressed as

$$Q_0 = \varphi_L(E_{hv} + \Delta H_{L-BR}) + (1 - \varphi_L)E_{hv} = E_{hv} + \varphi_L \Delta H_{L-BR} \tag{4}$$

where ϕ_L is the quantum yield of the BR* → L step and ΔH_{L-BR} is the enthalpy change (negative) from the L intermediate to the ground-state BR, which is observed with the 1 μs laser pulse. The external work done by the volume changes is negligible, and the energy of the proton movement across the molecule is dissipated on the microsecond time scale so we are justified in equating the heat energy and enthalpy changes.

For the following i steps

$$Q_i = -\varphi_i \Delta H_i \tag{5}$$

$$\Delta V_i = \varphi_i \Delta \bar{V}_i \tag{6}$$

where Q_i and ΔV_i are the observed heat release of the ith step directly from the fitting, ΔH_i and $\Delta \bar{V}_i$ are the molecular enthalpy and volume changes related to the observed values by the reaction yield ϕ_i. For a complete photocycle, we require and find $\sum_i Q_i = E_{hv}$ and $\sum_i \Delta V_i = 0$.

RESULTS AND DISCUSSION

Overview. Panels a and b of Figure 1 show the photopressure signal from the purple membrane and the reference upon illumination by a flash of light at two temperatures (25 and 2.5 °C). The fit of the former by an impulse component and three exponential components convolved with the reference is also shown as a thin solid line on the signal curve. The residuals of the fitting (trace C) are shown on the same figure with an expanded scale on the right axis. A small (<3%) slower component at 2.5 °C may also be present. The biphasic purple membrane signal at 25 °C, under all conditions, has a larger amplitude than the reference, indicating a positive volume change component, which is confirmed by the 2.5 °C trace. Figure 2 compares the kinetics at different pHs, and in different buffers at 2.5 °C. The fitting parameters are listed in Table 1. Only selected data at 25 and 2.5 °C (the magic temperature, i.e., the temperature of

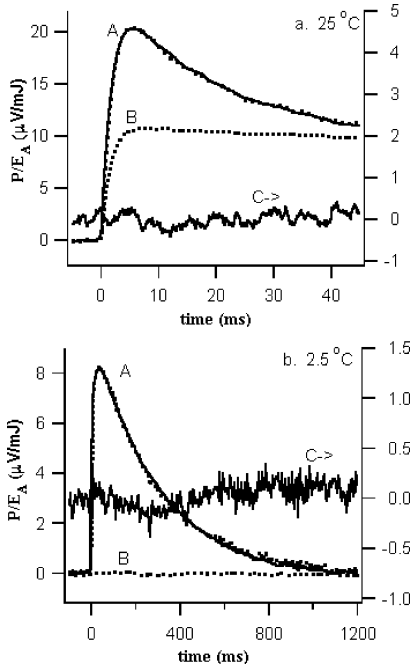

FIGURE 1: Photoinduced pressure changes in a purple membrane suspension or black ink reference at (a) 25 or (b) 2.5 °C (magic temperature): (A) dots for the purple membrane and solid line for the least-squares fit with three time constants, (B) reference, and (C) residues of the fitting (right scale). The fitting parameters for the data at 20 and 2.5 °C are listed in Table 1. Traces A and B are averages of 100 flashes. A positive signal reflects a positive volume change. The concentration of BR was approximately 40 μM. Both of the samples were in 10 mM phosphate buffer (pH 8.0) with a KCl concentration of 100 mM. The absorbance of the ink was equal to that of the purple membrane at the excitation wavelength of 585 nm.

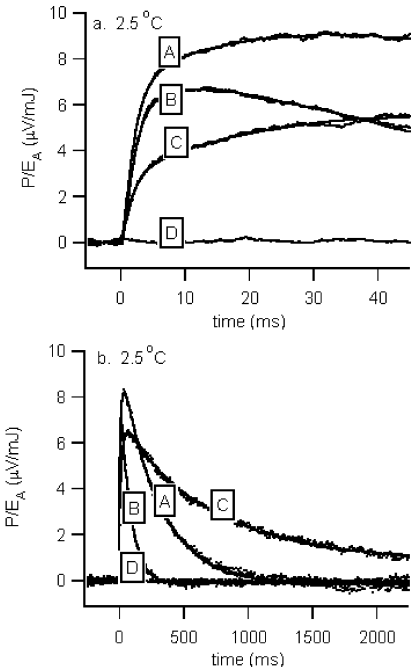

FIGURE 2: Photoinduced pressure changes in a purple membrane suspension or black ink reference at 2.5 °C (magic temperature) on a time scale of (a) 50 or (b) 2500 ms: (A) PM in phosphate buffer (pH 8.0), (B) PM in phosphate buffer (pH 7.0), (C) PM in Tris buffer (pH 8.4), and (D) reference. Thin solid lines are the fits with parameters listed in Table 1.

maximum density) are shown. The errors quoted are the result of a sensitivity analysis of the fitting parameters. Any single set of data can be fit with less error, but the global fit over the complete time scale increases the error while increasing self-consistency. This is because of the limited S/N ratio of these data and the relative insensitivity of some parameters to the least-squares control parameter. In this case, A_0 and A_3 are well-defined while A_1 and A_2 are less so. We used the best global fit as the deciding parameter. The plot of the amplitudes versus the normalized thermal expansivity in phosphate buffer at pH 8 (Figure 3) shows that the fast rise is largely a heat effect and the time-resolved components are largely volume changes (Table 2). The other data at pH 7 and with Tris buffer at pH 8.5 over the temperature range are similar. The linearity of the plots supports the assumption that ΔV and ΔH are temperature-independent over the temperature range of the experiment.

An objection could be made that our photopressure methodology has resolved only three components of the photocycle whereas the optical measurements are fit with models of at least four reversible and two irreversible steps (10 rate constants) and individual steps are being continually subdivided, now to nine steps (*12*). Some kinetic models proposed that parallel or branched photocycles of both proton pumping and non-proton pumping sequences could explain the experimental results as well as the model including only a single cycle but with reversible and irreversible steps (*8, 25*). Hendler has made elaborate calculated fits to available data and conducted a thorough review of all models (*26*). The conclusion is that no one model fits all data. It is clear that the problem cannot be resolved by the optical studies alone. What is required is independent input from FTIR, photoacoustics, and similar methods. We stress two points. First, the fact that there are more optically visible steps than actual proton transfer steps is not unexpected. The retinal chromophore is an excellent "reporter" group for any changes in its environment, whether or not they have directly to do with proton pumping. Only the proton transfers from and to the Schiff base will have a direct and large effect on the spectrum. Other proton transfers will have only indirect effects. Thus, the number of steps observed will be a function of the observational method. The time constants of these observed steps may not necessarily be identical, or even visible (*9*), in the various methodologies. Second, when one observes with more specific methods, such as FTIR, the number of observed time constants, within the signal-to-noise ratio, is reduced to two or three. This is seen, for example, in the data of Hessling et al. (*27*). Even the optical data can be summarized into three steps at the 80% relative concentration level in an alkaline solution (*10*). One must distinguish between the fits to the particular observed data and the complex global fits of the optical data with their myriad parameters. We are concerned with the former case.

The following observations are clear from our data.

(1) A long time after the flash, the pressure changes for the purple membrane (PM) samples and the ink reference are the same; i.e., after completion of the BR photocycle, the total heat released equals the energy of the photon [205 kJ/mol (Figure 1a)] and the total volume change is zero within error (Figure 1b), as shown in the last column of Table 2. These data are consistent with and are required for a complete photocycle with no energy storage in ion gradients.

Table 1: Fitting Parameters for eq 2, the Kinetic Data of the Direct Photopressure Measurements at 2.5 and 20 °C[a]

buffer	pH	temp (°C)	A_0	A_1	τ_1 (ms)	A_2	τ_2 (ms)	A_3	τ_3 (ms)	$\sum A_i$
phosphate	7.0	20	0.72	0.50	0.08	0.38	1.4	−0.80	9.6	0.80
		2.5	−0.06	0.51	0.6	0.20	12.5	−0.75	100	−0.06
phosphate	8.0	20	0.65	0.65	0.1	0.55	1.5	−1.0	33	0.80
		2.5	−0.03	0.53	0.6	0.43	22	−1.0	300	0.07
Tris	8.4	20	0.80	0.20	0.1	0.53	1.9	−0.66	63	0.87
		2.5	−0.08	0.23	0.4	0.36	22	−0.58	1500	0.06

[a] Buffer conditions: buffer concentration at 10 mM containing 100 mM KCl. The A values are in fractions of the reference amplitude. Signal filtering was decreased to 3 kHz to acquire the fast τ values. At 25 and 31 °C and pH 8, τ_1 is too fast to be well-determined so A_0 and A_1 cannot be separated (data not shown here). Since the data are normalized to 25 °C, the $\sum A_i$ value is expected to be 0.82 at 20 °C and 0 at 2.5 °C. The error is ±5%. Note that the data used to obtain values in Table 2 covered eight temperatures between 0 and 31 °C.

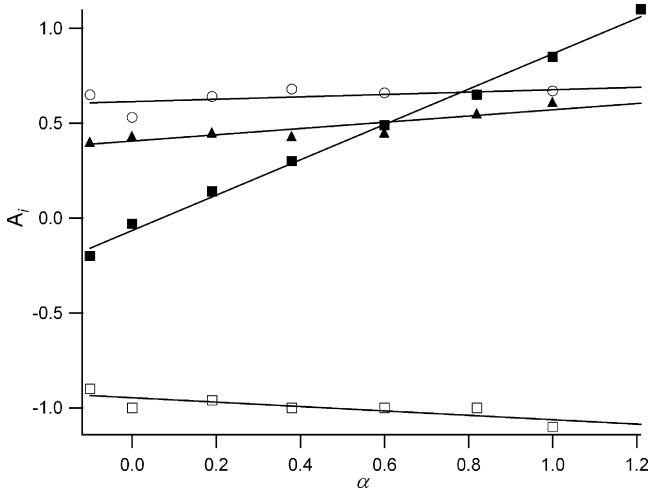

FIGURE 3: Amplitudes (normalized to the reference at $\alpha = 1$) of the photopressure changes A_i vs α'^T/α'^{25} with the A values for PM in 10 mM phosphate buffer (pH 8.0) and 100 mM KCl. The thin solid lines are the fitting to straight lines with eq 3. The fitting parameters are listed in Table 3: (■) A_0, (○) A_1, (▲) A_2, and (□) A_3.

(2) At the magic temperature of 2.5 °C where thermal expansivity $\alpha = 0$ (note that the magic temperature shifts from 4 °C in pure water to 2.5 °C, due to the presence of ~110 mM salt in the buffer), the pressure change in the ink reference disappears (Figure 2a,b, trace D). The transient pressure change of the purple membrane remains large and positive, but the rise and decay kinetics of the changes are slowed (Figure 2 and Table 1).

(3) Following photoexcitation at 2.5 °C, the volume of the purple membrane increases in two steps (Figure 2a). Both components of the expansion are kinetically first-order. The decay of the volume change is a single exponential (Figure 2b).

(4) The amplitudes of the faster expansion and the final decay depend on the ion of the buffer, indicating these proton transfer steps involve external protons (to and from the buffer species). The slower expansion (second step) depends much less on the buffer (Figure 2a, traces A and C, and Table 1), showing this is an internal change. The buffer ion has no large effect on the rate of the volume increases. However, pH plays a strong role in the decay kinetics (Figure 2b, traces A and B, and Table 1). The contraction becomes slower at higher pH because fewer protons are available for uptake. It is also noted that at 2.5 °C, the pH of the Tris buffer is ~9.2 (*28*), which may account for the slower decay in Tris buffer than in phosphate buffer (the pH of which is less dependent on temperature).

(5) There are substantial positive enthalpy changes (negative heats or cooling) at the slowest step but with appreciable errors. These positive enthalpies support the concept of entropically driven final steps in the BR photocycle (*1*).

Quantum Yield of Proton Pumping. Since all data are normalized to absorbed photons, each amplitude component is expressed in the form $\phi_i(\alpha'\Delta Q_i + \Delta V_i)$. Thus, knowledge of the reaction yields, ϕ_i, is required to obtain absolute molar values of ΔH_i and ΔV_i. Ort and Parson (*14*) used enthalpy and volume differences in different buffers, together with the known aqueous molar volume changes of protonation of phosphate dianion (+40 Å^3) and Tris (−1 Å^3) (*29*), to calibrate their instrument sensitivity and also to calculate the quantum yield of proton pumping. Yields of 0.25−0.42 were obtained depending on the photon flux and salt concentration. However, the calculations involved dividing differences in observed values by differences of differences (~3% of the observed values) and thus have severe, unstated errors.

Observed from our data, the increase in $\Delta\Delta V_1$ (+8.4 Å^3) with the change from Tris to phosphate buffer near pH 8 (Table 2) is small, the same as that observed by Ort and Parson. The inverse change in $\Delta\Delta V_3$ (−8.5 Å^3) is in good agreement for the deprotonation of the buffer. The direct interpretation of our data produces a quantum yield (ϕ) of 0.2, similar to that of Ort and Parson at low ionic strengths. We will discuss this assumption below.

We cannot apply the same argument to the values of ΔH using the heat of buffer protonation because of the relatively large errors in the observed enthalpy changes. For example, the difference in protonation enthalpies of phosphate (−7.5 kJ/mol) and of Tris (−48 kJ/mol) is +40 kJ/mol (*30*), while the observed difference (phosphate − Tris) in enthalpy changes $\Delta\Delta H_1$ is +10 ± 15 kJ/mol and $\Delta\Delta H_3$ is +2 ± 13 kJ/mol (Table 2). The expected values would be +8 and −8 kJ/mol if the quantum yield were 0.2. Though these value are still within the error range, we cannot determine the quantum yield from these data.

An alternative but not exclusive explanation of these low apparent yields is that buffer ions, particularly positive ions, are bound to the highly charged surfaces of the PM (*31, 32*). In that case, the ΔH values of protonation will be modified by the differences in the energy of binding of the buffer ions to the PM. The volume change by electrostriction is also expected to be sensitive to the position of the ion. The high local ionic strength at the binding sites will decrease the electrostriction, to one-half in the case of contact ion pairs of equal radii, because of overlapping electric fields. The presence of the nearby protein could slightly increase the level of electrostriction.

The quantum yield of the primary photoreaction (ϕ_K) has been a focus of conflicting arguments for more than a decade, but the high value of ~0.65 has been widely accepted since

Table 2: Observed Volume Changes (ΔV_i) and Heat Releases [Q_i ($\Delta H = -Q$)] of a Purple Membrane from the Fitting of Plots of A_i vs α'^T/α'^{25} As Shown in Figure 3 by eq 3[a]

buffer	pH	ΔV_0	ΔV_1	ΔV_2	ΔV_3	$\Sigma\Delta V_i$	ΔQ_0	ΔQ_1	ΔQ_2	ΔQ_3	ΣQ_i
phosphate	7.0	−1.3 (0.1)	10.8 (0.7)	5.7 (0.6)	−15.8 (0.5)	−0.6 (1.1)	+193 (2)	+18 (14)	+40 (10)	−31 (8)	+220 (19)
phosphate	8.0	−1.3 (0.5)	13.5 (0.7)	8.9 (0.5)	−20.8 (0.5)	0.3 (1.1)	+184 (9)	+14 (14)	+34 (8)	−24 (8)	+208 (20)
Tris	8.4	0.7 (0.3)	5.1 (0.5)	7.8 (0.1)	−12.3 (0.7)	1.3 (0.9)	+196 (7)	+4 (10)	+49 (2)	−26 (11)	+223 (17)

[a] The units for the ΔV_i values are cubic angstroms per photon, and the units for the ΔQ_i values are kilojoules per photon. The values in parentheses are the standard deviations of the fits. The theoretical values for $\Sigma\Delta V_i$ should be 0 and for $\Sigma\Delta Q_i$ should be 205 kJ/photon.

Table 3: $\phi\Delta H$ Data of This Work (errors of ±10 kJ/photon except for the error of ±6 for $\phi\Delta H_{L-BR}$) and Those Adapted from Ort and Parson (*1*), Varo and Lanyi (*44*), and Ludmann et al. (*10*)[a]

buffer	pH	ionic strength	$\phi\Delta H_{L-BR}$ at <50 μs	$\phi\Delta H_1$ at ~100 μs	$\phi\Delta H_2$ at ~1 ms	$\phi\Delta H_3$ at ~30 ms	method
phosphate	7.0	100 mM KCl, 10 mM buffer	−27	−18	−40	+31	photopressure
phosphate	8.0	100 mM KCl, 10 mM buffer	−24	−14	−34	+24	photopressure
Tris	8.4	100 mM KCl, 10 mM buffer	−27	−4	−49	+26	photopressure
pyrophosphate	8.5	200 mM KCl, 2 mM buffer	−23	−9	−50	+39	photopressure (*1*)
pyrophosphate	8.5	2 mM buffer alone	−29	−15	−50	+42	photopressure (*1*)
phosphate	7.0	100 mM NaCl, 50 mM buffer	NA	+10	−57	+36	temperature dependence of kinetics (*44*)
Tris	8.5	100 mM NaCl, 25 mM buffer	NA	−5	−15	+65	temperature dependence of kinetics (*10*)

[a] All in units of kilojoules per photon. The values from refs *10* and *44* have been calculated with a quantum yield of 0.65.

1990 (*33–37*). The yields of the following dark-thermal reactions are generally assumed to be 1. However, the yield of proton pumping of the photocycle may not be the same as that of the optical primary reaction. Very few absolute yields of proton pumping measurements can be found in the literature. Whole cells in 4.3 M NaCl have a yield of ~0.6 (*38, 39*). Govindjee et al. claimed a quantum yield of ~0.7 for PM in 0.5 M KCl and 0.25 in 0.01 M KCl (*40*). Korenbrot and Hwang found a yield of 0.65 proton per absorbed photon in oriented BR/lipid films in 5×10^{-4} M $NaHCO_3$ and 5×10^{-4} M $CdCl_2$ at pH 5.8 (*41*). Ionic conductivity showed a ϕ of 0.4 at pH 4 but could not be used at more alkaline pH, because the movement of several nonproton ions interferes with the measurements (*42, 43*). Thus, the quantum yield of the proton pumping could be smaller than the quantum yield of the primary step in the photocycle.

Because of these uncertainties in the yields, we present the data in observed, per absorbed photon, not molar, quantities.

Enthalpy Change, ΔH_i. The $\phi_i\Delta H_i$ values for each step i are simply the negative of the measured Q_i, listed in Table 3, together with some other previously published values for comparison. It is noted that the ΔH_2 values in the literature vary widely from −170 kJ/mol (*1*) (Ort and Parson, ϕ = 0.3, pyrophosphate, pH 8.5) to our value of −54 kJ/mol (ϕ = 0.65, phosphate, pH 8.0). This disagreement and similar disjunctions of other data are much ameliorated when the values are presented in the measured units of kilojoules per photon (Table 3). We believe that the variable, assumed quantum or reaction yields cause most of the disagreement in the literature.

Prompt Enthalpy Changes, ΔH_0. The prompt Q_0 accounts for ≥90% of the total heat change (Table 2) and thus the $\phi\Delta H_{L-BR}$; i.e., the difference in the enthalpy of the L state and the BR ground state is small. An enthalpy storage is observed in the L state, 26 ± 6 kJ/photon (Tables 2 and 3). On the time scale of <50 μs (our instrument resolution time), the prompt changes include BR* → K → L transitions. The initial relaxation of the photoexcited state involves all-trans to 13-cis isomerization of the retinal and concurrent changes in the protein. It is accepted that the enthalpy storage in the K intermediate is +20 to +40 kJ/mol (*33, 35, 44, 45*) with a quantum yield for K formation of ~0.65. The K → L transition has a very small enthalpy change (*45*); therefore, a heat release of ≥85% of the photon energy is expected upon formation of the L state (~1 μs).

Time-Resolved Enthalpy Changes, ΔH_i. The fast rise step has an enthalpy change $\phi\Delta H_1$ (L → M step) on average of −12 ± 13 kJ/photon (Table 3). The large errors in ΔH_1 and ΔH_0 are caused by the closeness of τ_1 to the resolution time and the decrease in the observed Q at lower temperatures as $\alpha \rightarrow 0$. Our ΔH_1 values agree within this error with the values of Ort and Parson (*1*) and Ludmann et al. (*10*) (Table 3). Varo and Lanyi (*44*) found a small but positive value. The latter two were obtained by analysis of the temperature variation of kinetics. These values, involving analysis of complex, multicomponent system (approximately five spectral forms and six to nine time constants), apply only to steps considered to be at equilibrium. They are difficult to compare with the direct measures in the simple three-step system. We may not be comparing truly similar steps. Further, in the latter papers, the concepts of quantum and reaction yields are replaced by those of "fraction cycling", with the assumption that reaction yields are unity. The fraction cycling was 25%, which implies that flux energies well into saturation were used. A possibility is that intermediate K was photoexcited causing unknown complications, e.g., photoreversals causing the appearance of "equilibria".

The slow rise component has an enthalpy change $\phi\Delta H_2$ (M → N step) of −37 ± 9 kJ/photon for phosphate at pH 7−8, which is some 30% smaller than that of Ort and Parson (*1*) and close to that of Varo and Lanyi (*44*) but larger than that of Ludmann et al. (*10*), yet within twice our estimated error (Table 3).

The $\phi\Delta H_3$ of the final step, N → O → BR, is positive, +27 ± 9 kJ/photon, under these three conditions and close to that of Ort and Parson (*1*) and of Varo and Lanyi (*44*) but smaller than that of Ludmann et al. (*10*) (Table 3). The reaction is entropy-driven as Ort and Parson claimed. The large positive enthalpies (and entropies) assigned to the N → O step by Ludmann et al. will not be visible in our

Table 4: $\phi\Delta\bar{V}$ per Photon Data of Our Work (errors of ±0.6 Å^3/photon) and Those Adapted from Ort and Parson (*13*), Varo and Lanyi (*56*), Klink et al. (*12*), Zhang and Mauzerall (*45*), Schulenberg et al. (*46, 57*)[a]

buffer	pH	ionic strength	$\phi\Delta\bar{V}_0$	$\phi\Delta\bar{V}_1$	$\phi\Delta\bar{V}_2$	$\phi\Delta\bar{V}_3$	method
phosphate	7.0	100 mM KCl, 10 mM buffer	−1.3	11	6	−16	photopressure
phosphate	8.0	100 mM KCl, 10 mM buffer	−1.3	14	9	−21	photopressure
Tris	8.4	100 mM KCl, 10 mM buffer	0.7	5	8	−12	photopressure
phosphate	7.4	50 mM KCl, 50 mM buffer	NA	16	6	−22	photopressure (*13*)
Tris	7.4	50 mM KCl, 50 mM buffer	NA	4	6	−10	photopressure (*13*)
CAPS	10.0	100 mM NaCl, 50 mM buffer	−17	5	33	−20	pressure dependence of kinetics (*56*)
Tris	7.0	150 mM NaCl, 15 mM buffer	−12	12	10	−6 (N → O)	pressure dependence of kinetics (*12*)
Tris	7.0	10 mM buffer	−1.1	NA	NA	NA	photoacoustic (*45*)
Tris	7.0	10 mM buffer	35	28	NA	−37	photothermal (*46, 57*) beam deflection

[a] All in units of cubic angstroms per photon (1 mL/Einstein = 1.66 Å^3/photon). Data reported in refs *12* and *56* have been corrected using a quantum yield of 0.65.

measurements because of the small amount of O present at pH 7−9. The small magnitude of O greatly increases the error of the molar values quoted by Ludmann et al. Neither of the papers on thermal effects of the kinetics has much discussion of error.

We note that in Ort and Parson's data analysis, the expansivity α of the medium, a nonlinear function of temperature, was neglected. Omitting this resulted in steeper slopes (∼20%) of both signs when the amplitude of volume change was plotted versus temperature. This could explain the discrepancy between our data and those of Ort and Parson. The presence of a large volume change can magnify the effects on the slope, leading to a larger ΔH_i (*24*). Together with a low quantum yield of ∼0.3, they thus calculated very large enthalpy changes per mole, of both signs.

Volume Changes: Prompt, ΔV_0, and Time-Resolved Volume Changes, ΔV_i. The volume changes of the BR cycle we obtained in this study and the data from the literature are summarized in Table 4. As an example of the variation of the data in the literature, the volume changes of the decay, ΔV_3 (when presented in units of cubic angstroms per mole), vary from −310 (*46*) ($\phi = 0.12$) and −32 (*13*) ($\phi = 0.3$) to our value of −18 ($\phi = 0.65$) in Tris (pH 7.0−8.4). But when they are expressed as $\phi\Delta V$, i.e., ΔV per photon, the overall agreement is striking, involving three different methodologies (Table 4).

The small observed ΔV_0 is consistent with the earlier photoacoustic results of Zhang and Mauzerall (*45*) and Logunov and El-Sayed (*36*). The values of Varo and Lanyi (*56*) and that of Klink et al. (*12*) are larger, but the comment on the difficulty of comparing data from analysis of thermal (here pressure) variation of spectral kinetics and our direct measures also applies here.

The values of ΔV_1 are remarkably consistent, with the exception of those of Schulenberg et al. (*46*). The same occurs with their value of ΔV_3.

The ΔV_2 of Varo and Lanyi (*56*) is some 4-fold larger than the other results which are in good agreement. The above comment on analysis of kinetic data applies here. Klink et al. (*12*) assigned volume changes to time-dependent processes of electrostriction involving reorientation of molecules, but reorientation of molecules does not per se produce a volume change. Electrostriction arises from the large electrostatic pressure (>10^4 atm) developed in the dielectric by the gradient of the electric field surrounding the ions. It occurs as fast as charge formation since it proceeds with the speed of sound and thus takes a few picoseconds for an average protein. It is quite possible that the protein structure relaxes following this shock, but we have no direct evidence of such processes. We do argue that the strain placed on the protein structure may well be an energy storage mechanism and the source of protein conformation changes.

Calculation of Volume Changes. The volume change in a proton transfer step can be explained by the electrostriction effect (see more details in the Supporting Information). Following our work on photosynthetic systems (*24, 47–50*), our approach is to explain as much as possible via electrostriction and then to resort to other contributions, such as volume conformational changes.

A definite conclusion is that the difference in the protonation volume change of the phosphate (P) and Tris (T) times the quantum yield is 8 ± 1 Å^3/photon. This leads to a ϕ of 0.21 ± 0.02 if the aqueous values for the buffers are used [the molecular volume change of protonation of phosphate, P, is +40 Å^3 and of Tris, T, is −2 Å^3 (*29*)], which was done by Ort and Parson (*14*). This assumption fails for the individual fits for ΔV_i (see the Supporting Information for details). However, the data can be fit with the accepted ϕ of 0.65 if the molar volume changes of protonation of phosphate (P) and Tris (T) are allowed to be different from the literature values, which could be caused by the buffer ions binding to BR. If ϕ is 0.65, the difference in volume change between protonation of phosphate and Tris must be +12 Å^3 per molecule. Our estimate of the ΔV of electrostriction for protonation of Tris using the Drude−Nernst equation (*51*) and a radius of 1 Å (the charge is localized on the N) is −6 Å^3, and that for the phosphate dianion (charge of −2 to −1) with a radius of 1.5 Å is +12 Å^3 for a P − T difference of +18 Å^3. The Drude−Nernst equation tends to give overly small values for very small or multiply charged ions in aqueous solution (*52*), most likely because of dielectric saturation (*53*). The formation of ion pairs of the charged species in the protein with the buffer ions will reduce the volume change of protonation. Clearly, our calculations are an approximation and are justified by their usefulness.

The results of these calculations (given in the Supporting Information) are summarized in Table 5. Our ΔV data can be accommodated quite well by what is known about the proton transfer pathway and with a semiquantitative interpretation based on electrostriction. We use our Drude−Nernst estimation of the molecular protonation volume change of +12 Å^3 for phosphate and −6 Å^3 for Tris to be self-consistent. We assume $\phi = 0.65$. The estimation of ΔV_1 depends on the model of the proton reaction complex (PRC) used. Data are shown for six PRC models in Table S1. The PRC models that give the acceptable fits are those (1) with

Table 5: Summary of Observed Volume Changes and Those Estimated via Changes in Electrostriction and Conformations[a]

step at 25 °C	optical	proton transfer reaction	$\Delta V_{calculated}$ Å^3 per molecule	$\Delta V_{observed}$ Å^3 per molecule
fast rise, 0.05 ms, ΔV_1	L → M	$SBH^+ \rightarrow D85^-$	+27	
		PRCH → BUF	$-15 + B$	
		total (assuming +12 for P and −6 for T)	+23.5 in phosphate, +5.5 in Tris	+21 in phosphate, +8 in Tris
slow rise, 1 ms, ΔV_2	M → N	D96H → SB	−37	
		D85 → PRC	+5	
		helix move	$C = +40$	+8
decay, 6 ms, ΔV_3	N → O and O → BR	$BUFH \rightarrow D96^-$	$+15.5 - B$	
		13-cis → trans	−2	
		helix return	−40	
		total	−38.5 in phosphate, –20.5 in Tris	−32 in phosphate, −18.5 in Tris

[a] Conditions: 10 mM buffer, pH 8, 100 mM KCl, ~40 μM BR. ϕ is assumed to be 0.65. ΔV values are in units of cubic angstroms per molecule. Abbreviations: SB, Schiff base; SBH^+, protonated SB; PRC, proton reaction complex; PRCH, protonated PRC; BUF, buffer; BUFH, protonated buffer; *B*, volume change of buffer protonation; *C*, conformational volume change; *P*, volume change of phosphate protonation; *T*, volume change of Tris protonation. The arrows in the third column link the starting group and the ending group of the proton. The volume change of the monoprotonated Glu or diglutamate with charge delocalization models for the PRCH is assumed. The estimated accumulated error is ±4 Å^3.

only one of the pair of glutamates protonated or (2) with two glutamate anions and an arginine cation with a proton and three water molecules with the charge totally delocalized over a 2.5 Å radius.

For the slow rise, ΔV_2, the proton transfer from Asp96 to the Schiff base creates charge with a necessarily negative volume change as does the loss of a proton from Asp85. The protonation of the PRC can approximately cancel one of the former three contractions. Thus, the estimation of ΔV_2, using the same value of the PRC as for ΔV_1, results in an expected change of −32 Å^3 (sum of –37 and +5). To account for the observed value of +8 Å^3, a positive conformational expansion of +40 Å^3 is required given a ϕ of 0.65. This is shown in the second row of Table 5. Our estimation of the volume change created by a small tilt of a helix, +60 Å^3, could easily account for this change (see the Supporting Information).

The estimation of ΔV_3 involves three proton transfer steps, but these involve the buffer, conformational changes, and a known small volume change of retinal isomerization. An important point for both our data and the fits is that they require closure of the cycle, i.e., $\sum \Delta V_i = 0$, which they do with a total error of −3 Å^3.

We note that the small observed and calculated ΔV values in each of the steps are caused by cancelation of large opposing changes occurring within the same time-resolved step (Table 5). This particular order may have been selected by evolution to reduce strain in the BR structure. The use of D_2O or a mutant which delays or speeds one of these pairs of processes would allow separation of these signals and thus give reliable estimates of the individual volume changes.

As we narrow these estimates of the electrostrictive volume changes, it will be possible to obtain the κ/ε factor in the Drude−Nernst equation. Since we can estimate κ from the effect of pressure on the spectra (*54*), we can determine an effective ε for the PM. The κ of BR has been measured by ultrasound, to be 23 Mbar^{-1} (*55*), similar to that estimated for the bacterial reaction center (*50*). Our present estimate of the effective ε in BR is ~8. The effective ε is a very useful parameter since it incorporates the integral of the spatially varying ε over all space. It may vary at the different sites because of the varying number and rigidity of water molecules. Using the effective ε, one can readily estimate the electrostatic free energies of the steps. By comparison to the observed enthalpies, we can estimate the entropic contribution to these reactions, as we have done with the photosynthetic electron transfer reactions (*24*).

CONCLUSIONS

(1) Positive enthalpy steps of +27 ± 15 kJ/photon are found for the decay step of the photocycle. This is evidence of an entropy-driven reaction as the last step of the cycle as claimed by Ort and Parson (*1*).

(2) Our estimates of ΔV via electrostriction are consistent with what is known of the proton pathway. The proton on the PRC is either on a glutamate or on a totally delocalized charged complex.

(3) The volume changes require a large positive conformational expansion in the slow rise time scale, the M → N step, and its recovery on the decay time scale. We fit the data with an electrostriction factor, κ/ε, smaller in BR than in photosynthetic reaction centers because of the presence of water in the proton conduction path.

ACKNOWLEDGMENT

We thank Ms. Irene Zielinski-Large for preparation of the BR.

SUPPORTING INFORMATION AVAILABLE

Details of the calculations. This material is available free of charge via the Internet at http://pubs.acs.org.

REFERENCES

1. Ort, D. R., and Parson, W. M. (1979) Enthalpy changes during the photochemical cycle of bacteriorhodopsin. *Biophys. J. 25*, 355–364.
2. Lanyi, J. K. (2004) Bacteriorhodopsin. *Annu. Rev. Physiol. 66*, 665–688.
3. Balashov, S. P. (2000) Protonation reactions and their coupling in bacteriorhodopsin. *Biochim. Biophys. Acta 1460*, 75–94.
4. Neutze, R., Pebay-Peyroula, E., Edman, K., Royant, A., Navarro, J., and Landau, E. M. (2002) Bacteriorhodopsin: A high-resolution structural view of vectorial proton transport. *Biochim. Biophys. Acta 1565*, 144–167.
5. Edmonds, B. W., and Leuke, H. (2004) Atomic resolution structures and the mechanism on ion pumping in bacteriorhodopsin. *Front. Biosci. 9*, 1556–1566.
6. Balashov, S. P., and Lanyi, J. K. (2006) Bacteriorhodopsin. *Microb. Biotechnol.,* 339–336.
7. Lanyi, J. K. (2006) Proton transfers in the bacteriorhodopsin photocycle. *Biochim. Biophys. Acta 1757*, 1012–1018.

8. Lanyi, J. K., and Varo, G. (1995) The photocycles of bacteriorhodopsin. *Isr. J. Chem. 35*, 365–385.
9. Chizhof, I., Chernavskii, D. S., Engelhard, M., Mueller, K.-H., Zubov, B. V., and Hess, B. (1996) Spectrally silent transitions in the bacteriorhodopsin photocycle. *Biophys. J. 71*, 2329–2345.
10. Ludmann, K., Gergely, C., and Varo, G. (1998) Kinetic and thermodynamic study of the bacteriorhodopsin photocycle over a wide pH range. *Biophys. J. 75*, 3110–3119.
11. Heberle, J. (2000) Proton transfer reactions across bacteriorhodopsin and along the membrane. *Biochim. Biophys. Acta 1458*, 135–147.
12. Klink, B. U., Winter, R., Engelhard, M., and Chizhov, I. (2002) Pressure dependence of the photocycle kinetics of bacteriorhodopsin. *Biophys. J. 83*, 3490–3498.
13. Ort, D. R., and Parson, W. M. (1978) Flash-induced volume changes of bacteriorhodopsin-containing membrane fragments and their relationship to proton movements and absorbance transients. *J. Biol. Chem. 253*, 6158–6164.
14. Ort, D. R., and Parson, W. M. (1979) The quantum yield of flash-induced proton release by bacteriorhodopsin-containing membrane fragments. *Biophys. J. 25*, 341–354.
15. Dencher, N. A., Dresselhaus, D., Zaccai, G., and Buldt, D. (1989) Structural changes in bacteriorhodopsin during proton translocation revealed by neutron diffraction. *Proc. Natl. Acad. Sci. U.S.A. 86*, 7876–7879.
16. Subramaniam, S., Lindahl, M., Bullough, P., Faruqi, A. R., Tittor, J., Oesterhelt, D., Brown, L., Lanyi, J., and Henderson, R. (1999) Protein conformational changes in the bacteriorhodopsin photocycle. *J. Mol. Biol. 287*, 145–161.
17. Radzwill, N., Gerwert, K., and Steinhoff, H.-J. (2001) Time resolved detection of transient movement of helices F and G in doubly spin-labeled bacteriorhodopsin. *Biophys. J. 80*, 2856–2866.
18. Oesterhelt, D., and Stoeckenius, W. (1974) Isolation of the cell membrane of *Halobactrium halobium* and its fragration into red and purple membrane. *Methods Enzymol. 31A*, 667–678.
19. Edens, G. J., Liu, Y., Grzymski, J., and Mauzerall, D. (2003) Pressure cell for time-resolved calorimetric measurements of photoinitiated reactions on the fractional miillisecond and longer time scale. *Rev. Sci. Instrum. 74*, 2523–2529.
20. Mauzerall, D., Liu, Y., Edens, G., and Grzymski, J. (2003) Measurement of enthalpy and volume changes in photoinitiated reactions on the ms timescale with a novel pressure cell. *Photochem. Photobiol. Sci. 2*, 788–790.
21. Mauzerall, D. (1970) Multiple excitations and reaction yields in photosynthetic systems. *Photochem. Photobiol. 29*, 169–170.
22. Feitelson, J., and Mauzerall, D. (1996) Photoacoustic evaluation of volume and entropy changes in energy and electron transfer. Triplet state porphyrin with oxygen and naphthoquinone-2-sulfonate. *J. Phys. Chem. 100*, 7698–7703.
23. Frost, A., and Pearson, R. G. (1953) Kinetics and mechanism. *A study of homogeneous chemical reactions*, John Wiley and Sons, New York.
24. Edens, G. J., Gunner, M. R., Xu, Q., and Mauzerall, D. (2000) The enthalpy and entropy of reaction for formation of P^+QA^- from excited reaction centers of *Rhodobacter sphaeroides*. *J. Am. Chem. Soc. 122*, 1479–1485.
25. Hendler, R. W., Shrager, R. I., and Bose, S. (2001) Theory and procedures for finding a correct kinetics model for the bacteriorhodopsin photocycle. *J. Phys. Chem. B 105*, 3319–3328.
26. Hendler, R. W. (2005) An apparent general solution for the kinetic models of the bacteriorhodopsin photocycle. *J. Phys. Chem. B 109*, 16515–16528.
27. Hessling, B., Souvignier, G., and Gewert, K. (1993) A model independent approach to assigning bacteriorhodopsin's intramolecular reactions to photocycle intermediates. *Biophys. J. 65*, 1929–1941.
28. Perrin, D. D., and Dempsey, B. (1974) In *Buffers for pH and Metal Ion Control*, John Wiley & Sons, New York.
29. Neuman, R. C., Kauzmann, W., and Zipp, A. (1973) Pressure dependence of weak acid ionization in aqueous buffers. *J. Phys. Chem. 77*, 2687–2691.
30. Harned, H. S., and Owen, B. B. (1943) In *Physical Chemistry of Electrolyte Solutions*, ACS Monograph Series 95, p 514, American Chemical Society, Washington, DC.
31. Toth-Boconadizfn, R., Der, A., and Keszthelyi, L. (2000) Buffer effects on electric signals of light-excited bacteriorhodopsin. *Biophys. J. 78*, 3170–3177.
32. Tuparev, N., Petkanchin, I. B., and Taneva, S. G. (2001) Buffer-induced changes of purple membrane surface electric properties: An electro-optical study. *Colloids Surf., B 20*, 145–153.
33. Birge, R. R., Cooper, T. M., Lawrence, A. F., Masthay, M. B., Zhang, C., and Zidovetzki, R. (1991) Revised assignment of energy storage in the primary photochemical event in bacteriorhodopsin. *J. Am. Chem. Soc. 113*, 4327–4328.
34. Govindjee, R., Balashov, S. P., and Ebrey, T. G. (1990) Quantum efficiency of the photochemical cycle of bacteriorhodopsin. *Biophys. J. 53*, 597–608.
35. Logunov, S. L., Song, L., and El-Sayed, M. A. (1994) pH dependence of the rate and quantum yield of the retinal photoisomerization in bacteriorhodopsin. *J. Phys. Chem. 98*, 10674–10677.
36. Logunov, S. L., and El-Sayed, M. A. (1997) Determination of the quantum yield of photoisomerization and energy content in the K-intermediate of bacteriorhodopsin photocycle and its mutants by the photoacoustic technique. *J. Phys. Chem. B 101*, 6629–6633.
37. Logunov, S. L., El-Sayed, M. A., Song, L., and Lanyi, J. K. (1996) Photoisomerization quantum yield and apparent energy content of the K-intermediate of in the photocycle of bacteriorhodopsin, its mutants D85N, R82Q and D212N, and deionized blue bacteriorhodopsin. *J. Phys. Chem. 100*, 2391–2398.
38. Bogomolni, R. A., Baker, R. A., Lozier, R. H., and Stoeckenius, W. (1980) Action spectrum and quantum efficiency for proton pumping in halobacterium halobium. *Biochemistry 19*, 2152–2159.
39. Renard, H., and Delmelle, M. (1980) Quantum efficiency of light-driven proton extrusion in *Halobacterium halobium*: pH dependence. *Biophys. J. 32*, 993–1006.
40. Govindjee, R., Ebbrey, T. G., and Crofts, A. R. (1980) The quantum efficiency of proton pumping by the purple membrane of *Halobacterium halobium*. *Biophys. J. 30*, 231–242.
41. Korenbrot, J. I., and Hwang, S.-B. (1980) Proton transport by bacteriorhodopsin in planar membranes assembled from air-water interface films. *J. Gen. Physiol. 76*, 649–682.
42. Marinetti, T., and Mauzerall, D. (1983) Absolute quantum yields and proof of proton and nonproton transient release and uptake in photoexcited bacteriorhodopsin. *Proc. Natl. Acad. Sci. U.S.A. 80*, 178–180.
43. Marinetti, T. (1987) Abrupt onset of large scale nonproton ion release in purple membranes caused by increasing pH or ionic strength. *Biophys. J. 51*, 875–881.
44. Varo, G., and Lanyi, J. K. (1991) Thermodynamics and energy coupling in the bacteriorhodopsin photocycle. *Biochemistry 30*, 5016–5022.
45. Zhang, D., and Mauzerall, D. (1996) Volume and enthalpy changes in the early steps of bacteriorhodopsin photocycle studied by the time-resolved photoacoustics. *Biophys. J. 71*, 381–388.
46. Schulenberg, P. J., Gartner, W., and Braslavsky, S. E. (1995) Time-resolved volume changes during the bacteriorhodopsin photocycle: A photothermal beam deflection study. *J. Phys. Chem. 99*, 9617–9624.
47. Mauzerall, D., Gunner, M. R., and Zhang, J. W. (1995) Volume contraction on photoexcitation of the reaction center from *Rhodobacter sphaeroides* R-26: Internal probe of dielectrics. *Biophys. J. 68*, 275–280.
48. Hou, J. M., Boichenko, V., Wang, Y.-C., Chitnis, P. R., and Mauzerall, D. (2001) Thermodynamics of electron-transfer on oxygenic photosynthetic reaction centers: A pulsed photoacoustic study of electron transfer in photosystem I reveals a similarity to bacterial reaction centers in both volume change and entropy. *Biochemistry 40*, 7109–7116.
49. Hou, H. J. M., and Mauzerall, D. (2006) The A^-F_x to $F_{A/B}$ step in *Synechocystis* 6803 photosystem I is entropy driven. *J. Am. Chem. Soc. 128*, 1580–1586.
50. Mauzerall, D., Hou, J.-M., and Boichenko, V. A. (2002) Volume changes and electrostriction in primary photoreactions of various photosynthetic systems: Estimation of dielectric coefficient in bacterial reaction centers and of the observed volume changes with the Drude-Nernst equation. *Photosynth. Res. 74*, 173–180.
51. Drude, P., and Nernst, W. Z. (1894) Uber elektrostiktion durch freie ionen. *Z. Phys. Chem. 15*, 79–85.
52. Millero, F. J. (1971) The molal volumes of electrolytes. *Chem. Rev. 71*, 147–176.
53. Feitelson, J., and Mauzerall, D. (2002) Enthalpy and electrostriction in the electron transfer reaction between triplet zinc uroporphyrin and ferricyanide. *J. Phys. Chem. B 106*, 9674–9678.
54. Tars, M., Ellervee, A., Kukk, P., Laisaar, A., Saarnak, A., and Freiberg., A. (1994) Photosynthetic proteins under high pressure. *Liet. Fiz. Z. (1993-1999) 34*, 320–328.

55. Marque, J., Eisenstein, L., Gratton, E., Sturtevant, J. M., and Hardy, C. J. (1984) Thermodynamic properties of purple membrane. *Biophys. J. 46*, 567–572.
56. Varo, G., and Lanyi, J. K. (1995) Effects of hydrostatic pressure on the kinetics reveal a volume increase during the bacteriorhodopsin photocycle. *Biochemistry 34*, 12161–12169.
57. Schulenberg, P. J., Rohr, Gartner, M. W., and Braslavsky, S. E. (1994) Photoinduced volume changes associated with the early transformations of bacteriorhodopsin: A laser-induced optoacoustic spectroscopy study. *Biophys. J. 66*, 838–843.

BI800158X